LANGMUIR

Article

pubs.acs.org/Langmuir

Molecular Structure and Dynamics of Ionic Liquids in a Rigid-Rod Polyanion-Based Ion Gel

Zhou Yu,[†] Yadong He,[†] Ying Wang,[‡] Louis A. Madsen,*[,‡] and Rui Qiao*[,†]

[†]Department of Mechanical Engineering and [‡]Department of Chemistry and Macromolecules Innovation Institute, Virginia Tech, Blacksburg, Virginia 24061, United States

Supporting Information

ABSTRACT: The recent fabrication of liquid crystalline ion gels featuring rigid-rod polyanions aligned within room-temperature ionic liquids (RTILs) opens up exciting new avenues for engineering ion conducting materials. These gels exhibit an unusual combination of properties including high ionic conductivity, distinct transport anisotropy, and widely tunable elastic modulus. Using molecular simulations, we study the structure and dynamics of the ions in an ion gel consisting of rigid-rod polyanions and $[C_2mim][TfO]$ RTILs. We show that the ion distribution in the interstitial space between polymer rods exhibits the hallmarks of the RTIL structure near charged surfaces; i.e., cations (C_2mim^+) and anions (TfO^-) form alternating layers around the polymer rods and the charge on the rod is overscreened by the ionic layer surrounding it. The distinct ordering of ions suggests the formation of a long-range "electrostatic network" in the ion gel, which may contribute to its mechanical cohesion and high modulus. The dynamics of both C_2mim^+ and TfO^- ions slow down due to the fact that some C_2mim^+ ions become associated with the sulfonate groups of the polymer rod on nanosecond time scales, which hinders the dynamics of all ions in the gel. C_2mim^+ and TfO^- ion diffusion in the gel are only 2−10 times slower than in bulk RTILs, which is still much faster than, e.g., Li ions in typical ion conducting polymers. This fast ion transport combined with strong mechanical cohesion open up exciting opportunities for application of these gels in electrochemical devices including Li-metal batteries.

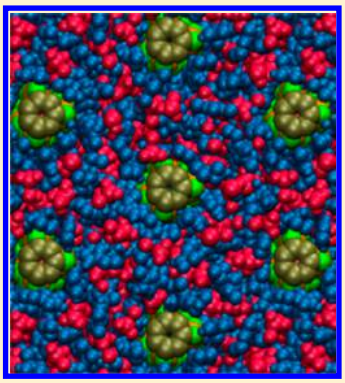

1. INTRODUCTION

Polymer electrolyte materials play a critical role in numerous applications including fuel cells, solar cells, and rechargeable batteries.[1,2] These applications often demand high ionic conductivity, mechanical strength and stiffness, and excellent thermal stability.[3,4] However, despite intensive research in the past decades, few existing materials can meet these demands simultaneously. In recent years, ion gels, polymeric networks swollen by room-temperature ionic liquids (RTILs), have shown great promise in meeting these demands.[5] RTILs are electrolytes that are composed entirely of ions but remain in the liquid state at relatively low temperature (e.g., <100 °C).[6] Many RTILs exhibit excellent ionic conductivity, electrochemical stability, and thermal stability.[7−9] Therefore, when RTILs are combined with suitable polymers, the resulting ion gels can provide many of the electrical, thermal, and mechanical properties desired for polymer electrolyte materials.[10−15] A recent breakthrough in this field is the synthesis of liquid crystalline gels containing a rigid-rod polyanionic aramid poly(2,2′-disulfonyl-4,4′-benzidine terephthalamide (abbreviated PBDT) and a RTIL 1-ethyl-3-methyl imidazolium trifluoromethane sulfonate ($[C_2mim][TfO]$).[16] These gels exhibit high ionic conductivity (up to 8 $mS{\cdot}cm^{-1}$ at room-temperature), widely tunable modulus (0.003−3 GPa), excellent thermal stability (up to 300 °C), and transport anisotropy (up to 3.5×). The fabrication of this ion gel opens up exciting new avenues for engineering polymer electrolyte materials. Given the flexibility of the molecular design of RTILs and ionic polymers, one can expect to even further improve both the ionic transport and mechanical properties of this type of ion gels through judicious selection of RTILs and polymers. Such rational design, however, demands a fundamental understanding of the structure and dynamics properties of the RTILs in the gel.

The structure and dynamics of RTILs in various systems have been studied intensely in recent years. First, in bulk RTILs, cation−anion interactions are strong and thus each ion effectively resides in a cage formed by its neighbor ions. The hydrophobic tails of cations can aggregate to form spatially heterogeneous domains.[17,18] The dynamics of ions also exhibit heterogeneity, with some ions diffusing considerably faster than other ions.[19,20] The diffusion of an ion in RTILs is strongly affected by the cage surrounding it: at short time when the ion has not yet escaped from its cage, ion diffusion is in the ballistic and then subdiffusive regime; at large time scale when the cage is broken due to cleavage by other ions, ion diffusion reaches the diffusive regime.[19,21−23] Second, for RTILs confined in planar or cylindrical nanopores, similar to most liquids, significant layering of RTILs occurs near the pore walls.[9] When the pore walls are charged, counterions and co-ions form

Received: October 18, 2016
Revised: December 5, 2016
Published: December 7, 2016

DOI: 10.1021/acs.langmuir.6b03798
Langmuir 2017, 33, 322−331

alternating layers near the wall. Except when the wall is very highly charged, the wall charge is overscreened by the first ionic layer near the pore wall.[9,24,25] The dynamic properties of ions vary notably across the pore, with the diffusion of the ions adjacent to the pore wall typically being slowest.[23,26] While the dynamics of ions are usually slowed down by confinement, sometimes the diffusion of ions inside the pore can be much faster than in the bulk,[27,28] e.g., when ion density inside subnanometer pores becomes notably smaller than that of bulk RTILs.[28] Finally, for RTILs in polymer membranes, most work has focused on the situation when RTILs are mixed with disordered polymers such as poly(ethylene oxide), and usually lithium salts such as lithium-bis(trifluoro-methane) sulfonamide were also included.[18,29−32] The local structure of ion pairing in polymer membranes exhibits a similar pattern as in bulk RTILs, though the imidazolium cations are also found to be partly solvated by polymer chains.[18] The dynamics of the imidazolium cations are notably slowed down by the polymers.[30] The RTILs can modify the conformation of the polymers and enhance their segmental dynamics compared to that in polymer lithium salt mixtures.[31]

These above prior studies of RTILs are a useful starting point for understanding the structure and dynamics of the RTILs in the ion gels developed in ref 16. Nevertheless, the RTILs in these new gels exist in rather different environments compared to those examined in the prior studies. Importantly, unlike those in bulk liquids, nanopores, or neutral polymer membranes, the RTILs in these gels are confined between rod-like, mobile but largely ordered polyanions with discrete charge moieties. Furthermore, the polyanion has a hydrophobic backbone and a radius that is comparable to the ion size. The structure and dynamics of RTILs in such a heterogeneous, confined environment cannot be simply extrapolated from the results obtained in other systems, and many questions about these properties remain open. For example, how do cations and anions organize around the polyanions? What are their dynamics? How are these dynamics related to the ion distribution near the polyanions, and ultimately the mass fraction of polyanions and the presence of metal ion impurities in the gel? In this work, we address these questions through molecular dynamics (MD) simulations using the PBDT-[C_2mim][TfO] ion gels as a model system. Given that the study this type of gel is still at the earliest stage, we focus on revealing the essential features of RTIL structure and dynamics in the gel rather than quantitatively reproducing experimental measurables such as the ion diffusion coefficients. The rest of the paper is organized as follows. The simulation system, model, and methods are presented in section 2; results on the structure and dynamics of the ions between PBDT rods are presented in section 3. Finally, conclusions are presented in section 4.

2. SIMULATION SYSTEM, MOLECULAR MODELS, AND METHODS

Since these sulfonated aramid-based ion gels are new,[16] we first outline the method for fabricating them before describing how they are simulated in this work. PBDT is a rigid-rod polyelectrolyte with high ion density along its backbone. PBDT forms a lyotropic liquid crystalline (LC) phase above a critical mass concentration of 1.2 wt %.[33] To make ion gels, an aqueous seed solution containing the polyanion PBDT and Na^+ counterions is placed inside a test tube and subjected to a magnetic field applied along the tube axis.[16] [C_2mim][TfO] liquids are then placed above the seed solution. Driven by processes including the ion and water exchange between the seed solution and the RTILs, ion gels form at the bottom of the test tube. The as-formed gel is then heated under vacuum to remove the water inside it. X-ray diffraction shows that the PBDT polyanions are highly ordered in the dried gel and RTILs are dispersed within the aligned PBDT matrix. Experimental nuclear magnetic resonance (NMR) measurements show that approximately half of the Na^+ ions in the seed solution remain in the dried ion gel when using the fabrication procedure of ref 16. The amount of residual Na^+ ions further depends on parameters that include the mass fraction of PBDT in the seed solution and the relative volume of the seed solution and the RTIL. Supporting Information section 9 describes NMR measurements to quantify Na^+ content in the ion gels.

2.1. MD System. Based on the ion gel structure measured experimentally, a molecular simulation system was developed. Figure 1 shows that the system consists of four rigid rods representing PBDT polyanions and the accompanying RTILs (in some cases, residual Na^+ ions were also added, see Table 1). In reality, each PBDT rod is tens of nanometers in length, too long to be modeled in MD simulations. Here each rod is 6.72 nm long. Initially, all rods are perfectly aligned in the z-direction. The simulation system is periodic in all three directions. These rods, together with their periodic images, form a hexagonal lattice in the xy-plane (see Figure S1 in the Supporting Information). The spacing between adjacent rods is denoted as S_{r-r}. The number of C_2mim$^+$ and TfO$^-$ ions was chosen to ensure the overall electroneutrality of the system. Initially, two slabs of RTILs were placed in contact with the two ends of the rods and a vacuum space was placed between the RTIL slabs (see Figure 1b). To obtain an ion gel, we fixed the rods and performed an NVT run for the RTILs to enter the space between the rods. This pre-equilibration process ends when the rods become fully wetted by RTILs and the number of RTIL molecules between the PBDT rods no longer changes (This typically takes less than 20 ns. See Figure S2 for the evolution of the number of RTIL molecules between PBDT rods when S_{r-r} is 2.2 nm). The PBDT rods and the RTILs between them obtained at the end of the equilibration process are considered as a model ion gel (see Figure 1b). We verified that the ion gel thus formed is electrically neutral. Ion gels with different mass fraction of PBDT were obtained by using different initial rod−rod spacing S_{r-r} during the above pre-equilibration

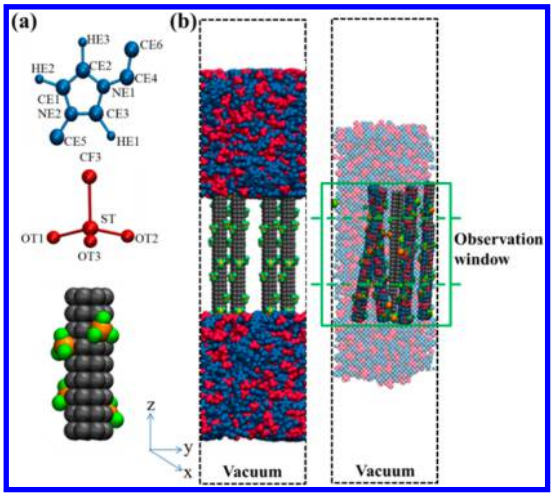

Figure 1. Molecular models of the PBDT-RTIL gel. (a) Structure of the C_2mim$^+$, TfO$^-$, and the semi-coarse-grained PBDT rod. Each rod consists of four chemical repeat units of PBDT. Orange (green) balls denote the sulfur (oxygen) atoms of PBDT sulfonate groups. (b) Snapshots of the system at the beginning and the end of the pre-equilibration process. The thin black dashed lines denote the simulation box, which is periodic in all three directions. The solid green lines enclose the model ion gel. The space between the two dashed green lines denotes the "observation window" in which the structure and dynamics of the RTILs were analyzed.

DOI: 10.1021/acs.langmuir.6b03798
Langmuir 2017, 33, 322−331

Table 1. Properties of the Equilibrated Ion Gel Systems Studied in This Work

system	nominal rod−rod spacing[a]	PBDT mass fraction	C_2mim^+/SO_3^- ratio	TfO^-/SO_3^- ratio	Na^+/SO_3^- ratio	lateral size, $L_x \times L_y$
1	2.0 nm	19.6%	4.45	3.21	0.0	3.46 × 4.00 nm^2
2	2.2 nm	16.3%	5.39	4.18	0.0	3.81 × 4.40 nm^2
3	2.2 nm	16.1%	5.05	4.47	0.5	3.81 × 4.40 nm^2
4	2.4 nm	13.8%	6.41	5.21	0.0	4.16 × 4.80 nm^2
5	2.8 nm	10.1%	8.74	7.65	0.0	4.85 × 5.60 nm^2

[a]This is taken as the rod−rod spacing during the pre-equilibration process, when perfectly aligned PBDT rods were fixed and formed a hexagonal lattice in the *xy*-plane.

process. Table 1 summarizes the various ion gels studied in the present work.

2.2. Molecular Models. C_2mim^+ and TfO^- ions were modeled using united-atom force fields,[34] in which the net charge of each ion was scaled to 0.8 e. These force fields were chosen as a compromise between computational cost and accuracy. Specifically, while these force fields are less rigorous compared to the polarizable force fields,[35,36] they enable the structure and dynamics of RTILs to be simulated relatively accurately with greatly reduced computational cost. For example, based on these force fields, our simulations of bulk [C_2mim][TfO] at 353 K and 1 atm predict a diffusion coefficient of 22.0 × 10^{-11} m^2/s for the C_2mim^+ and 12.1 × 10^{-11} m^2/s for the TfO^- ions, which agree quite well with those measured using NMR (17.5 × 10^{-11} m^2/s for the C_2mim^+ ion and 12.5 × 10^{-11} m^2/s for the TfO^- ions). In addition, prior studies indicated that simulations based on this type of force fields can capture the structure of interfacial RTILs (e.g., those near electrode surfaces) quite well.[37] The force fields for the sodium ions were taken from the OPLS-AA force field.[38]

The precise structure of the PBDT rods in the ion gel has not yet been fully clarified. Prior studies suggested that PBDT molecules self-assemble into rigid-rod building blocks in the form of double helix,[16,33] and such structure should persist in the ion gel. With the dimensions of the PBDT building block and the distribution of sulfonate groups on the rod inferred from X-ray diffraction data,[16] we built a semi-coarse-grained model for the PBDT polyanions. These polyanions were modeled as rigid rods decorated with explicitly resolved sulfonate groups (see Figure 1b). Each rod is 6.72 nm long and consists of four 1.68 nm-long repeating units. Each repeating unit (see Figure 1a) is further made of 9 layers of carbon atoms arranged into a regular heptagon (side length: 0.173 nm), and the spacing between adjacent carbon layers is 0.21 nm. Each repeating unit has four sulfonate groups anchored on the carbon atoms in different layers, and these units were stacked onto each other in a way that produced a helical pattern of the sulfonate groups on the PBDT rod (see Figures 1b and S3). The force field parameters for the carbon atoms and the sulfonate groups were taken from the OPLS-AA force fields, and are summarized in the Table S1. Because the objective of the present study is to delineate the essential features of the structure and dynamics of RTILs in ion gels and the precise structure of PBDT is not fully elucidated yet, the above molecular model is deemed a reasonable choice for several reasons. First, it captures the key chemical features of the PBDT rod including its semirigid structure, the hydrophobic nature of its backbone, and the discrete distribution of charge groups on the rod. By resolving the sulfonate groups explicitly, it also allows the strong interactions between the sulfonate groups and RTILs, which can greatly affect the structure and dynamics RTILs, to be modeled in detail. Second, by adopting a simple model for the PBDT rods with well-defined geometry, it facilitates the parametric study of how gel design parameters such as the PBDT mass fraction affects the properties of RTILs in the gel. Finally, the semi-coarse-grained model allows large system to be simulated for relatively long time period, which is necessary in the study of RTIL dynamics.

2.3. Simulation and Analysis Methods. Simulations were performed using the Gromacs code.[39] All simulations were executed in the NVT ensemble. The temperature of the RTILs was maintained at 353.15 K using the velocity rescaling thermostat.[40] The elevated temperature chosen here helps to achieve good statistics of ion displacement. After the pre-equilibration process described above, each system was further equilibrated for another 20 ns (except for a few selected cases, the PDBT rods were allowed to move during this equilibration step). This was followed by a production run of 80 ns. Table 1 lists the composition of the equilibrated ion gel systems studied in this work. A detailed list of the number of ions in each system (including those outside of the observation window shown in Figure 1b) is shown in Table S2 in the Supporting Information.

In the MD simulations, the nonelectrostatic interactions were computed by direct summation with a cutoff length of 1.2 nm. The electrostatic interactions were computed using the Particle Mesh Ewald (PME) method. The real space cutoff and FFT spacing were 1.2 and 0.12 nm, respectively. All bonded interactions were computed except that the length of the C−H bonds were constrained using the LINCS algorithm.[41] Note that to ensure the rigidity of the PBDT rod, strong harmonic bonds (bond constant: 5 × 10^6 kJ/(mol·nm^2)) were imposed between carbon atoms in different carbon layers and repeating units.

The trajectories of the system were saved during the production run. To avoid edge effects, only the RTILs in the middle portion of the ion gel (marked out as the "observation window" in Figure 1b) were considered in the analysis of the structure and dynamics of the RTILs. Since most PBDT rods were found to be aligned very well along the *z*-axis even when they were allowed to move, the ion diffusion coefficient in the perpendicular-to-rod direction was computed using $D_\perp = \lim_{t\to\infty} \mathrm{MSD}_{xy}(t)/4t$. $\mathrm{MSD}_{xy}(t)$ is the ion mean-square displacement in the *xy*-plane given by $\mathrm{MSD}_{xy}(t) = \langle (x_i(t) - x_i(0))^2 + (y_i(t) - y_i(0))^2 \rangle$, where x_i and y_i are the *x*- and *y*-position of ion *i*, respectively. $\langle \cdots \rangle$ denotes the ensemble average. The diffusion coefficient in the direction along the PBDT rods was computed using $D_\parallel = \lim_{t\to\infty} \mathrm{MSD}_z(t)/2t$. $\mathrm{MSD}_z(t)$ is the ion mean-square displacement in the *z*-direction given by $\mathrm{MSD}_z(t) = \langle (z_i(t) - z_i(0))^2 \rangle$, where z_i is the *z*-position of ion *i*. To determine the error bars for $D_\parallel$ and $D_\perp$ (denoted using $\varepsilon_{D_\perp}$ and $\varepsilon_{D_\parallel}$), we first computed the MSDs for five different time periods of the ion trajectory. $\varepsilon_{D_\perp}$ and $\varepsilon_{D_\parallel}$ were then calculated as the standard deviation of the diffusion coefficients obtained from MSDs. The error bar of $D_\parallel/D_\perp$ was obtained using $\varepsilon(D_\parallel/D_\perp) \approx |D_\parallel|/|D_\perp|^2 \varepsilon_{D_\perp} + |D_\perp|^{-1} \varepsilon_{D_\parallel}$. We note that the finite size of simulation box can potentially affect the value of computed diffusion coefficient.[42] Such a finite size effect is expected to be small in the system we are studying here. This is because the hydrodynamic interactions, which are responsible for finite size effects in the calculation of dynamic properties (e.g., diffusion coefficient) in MD simulations, are strongly screened by the PBDT rods in our system.

3. RESULTS AND DISCUSSION

3.1. Structure of Ionic Liquids in Ion Gels. Near extended surfaces, RTILs exhibit distinct structures at intermolecular and larger (e.g., intersurface) scales.[9,25,43] These structures and their response to external stimuli (e.g., a change of the distance between extended surfaces) often control macroscale observables such as the interactions between extended surfaces. In our ion gels,[16] distinct structures of RTILs should also develop, both at inter-rod and intermolecular scales. The structure of RTILs at the inter-rod

DOI: 10.1021/acs.langmuir.6b03798
Langmuir 2017, 33, 322−331

scale likely plays a key role in controlling the interactions between the polyanions and thus ultimately the mechanical and transport properties of the ion gel. Quantifying the structure of RTILs at this scale is complicated: although PBDT polyanions are highly ordered, there exist small variations in their orientation and their separation from other PBDT polyanions, and hence the RTIL structure must in principle be quantified between all PBDT polyanions simultaneously. To circumvent this complexity, we first consider the RTIL structure in a special case, in which perfectly aligned PBDT polyanions were arranged into a hexagonal lattice and fixed throughout the simulation. Figure 2 shows the distribution of C_2mim^+ and

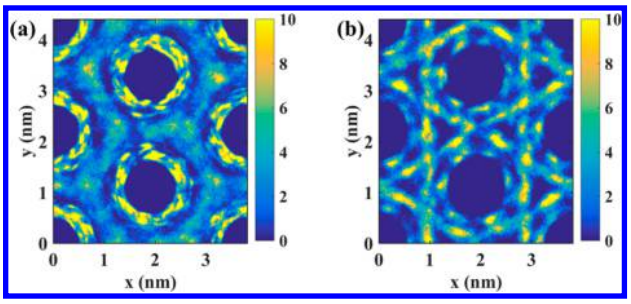

Figure 2. Density distribution of C_2mim^+ (a) and TfO^- ions (b) in the interstitial space between the PBDT polyanions in an ion gel. PBDT rods are fixed into a hexagonal lattice in the simulation, and the rod spacing is 2.2 nm. The ion density is color-coded, and the unit of the colorbar is nm^{-3}.

TfO^- ions in the interstitial space between PBDT rods when the rod−rod distance is 2.2 nm. A layer of C_2mim^+ ions adsorb on the surface of the negatively charged PBDT rods. The adsorption of these ions is not uniform along the rod's circumference because the sulfonate groups are distributed discretely on the PBDT rod. Some TfO^- ions are also found on the rod's surface. Visualization of the trajectories revealed that these anions are in contact with the PBDT rod's hydrophobic backbone, and they are partially shielded from the sulfonate groups by the C_2mim^+ ions solvating these groups. The first cation layer around the PBDT rod is further surrounded by a layer of TfO^- ions. These TfO^- ions form a hexagonal pattern, reflecting the pattern for the arrangement of PBDT rods. Hence, at a rod−rod separation of 2.2 nm (or equivalently, a PBDT mass fraction of ∼16% in the gel), the distribution of ions not immediately adjacent to the PBDT rods are already heavily affected by the packing of the PBDT rods. Finally, Figure 2 also shows that very few ion can reach a distance ≲0.5 nm from the rod's axis. Using the surface area of a cylinder with a radius of 0.5 nm and the charge on the PBDT rod (−2.38 e/nm), the effective surface charge density of the PBDT rod is determined as −0.12 C/m^2.

The inter-rod structure of RTILs shown in Figure 2 also exists when the PBDT rods are mobile (hereafter all results were obtained from simulations with mobile PBDT rods). Figure 3a shows the average ion density as a function of distance from the PBDT rod axis. The RTIL structures revealed here are similar to those shown in Figure 2: C_2mim^+ ions and TfO^- ions form alternating layers near the rod and some TfO^- ions appear at positions next to the PBDT rods' surface. The former is a hallmark of the distribution of RTILs near charged surfaces.[9,26,28] The latter is consistent with the anion concentration distribution shown in Figure 2 but rarely reported in studies of RTILs near solid surfaces with similar charge densities.[44] The notable adsorption of anions on surfaces occurs because, unlike in prior studies where charges are distributed uniformly on surfaces, here charges are distributed discretely along the PBDT rod in the form of sulfonate groups and there is space between these groups. This space is occupied primarily by the cations. However, some anions can also access this intercation area since their repulsive electrostatic interactions with the sulfonate groups are partially compensated by their attractive interactions with the cations adsorbed on the rod's surface.

To explore how RTILs screen the charge of the PBDT rods, we computed the charge screening factor β as a function of radial distance r from the rod axis[44]

$$\beta(r) = -\frac{1}{q_L}\int_0^r 2\pi r \rho_e(s)\mathrm{d}s \tag{1}$$

where $\rho_e(s)$ is space charge density due to ions at a radial distance s and q_L is the charge on the PBDT rod per unit length (−2.38 e/nm). At positions with $\beta > 1.0$, the surface charge on the rod is overscreened. Charge overscreening is a universal feature of the electrical double layers at the interfaces of RTILs and surfaces with low to moderate charge densities.[9,24] Figure 3b confirms that charge overscreening also occurs near PBDT rods. Since charge overscreening often leads to attractions between like-charged surfaces or polyelectrolytes,[45] the results shown in Figure 3b may help explain the mechanical strength of the ion gel studied here. Exploring the relation between charge overscreening (or more broadly, the RTIL structure in ion gels) and collective ionic interactions between charged rods and RTILs will form the basis of future studies.

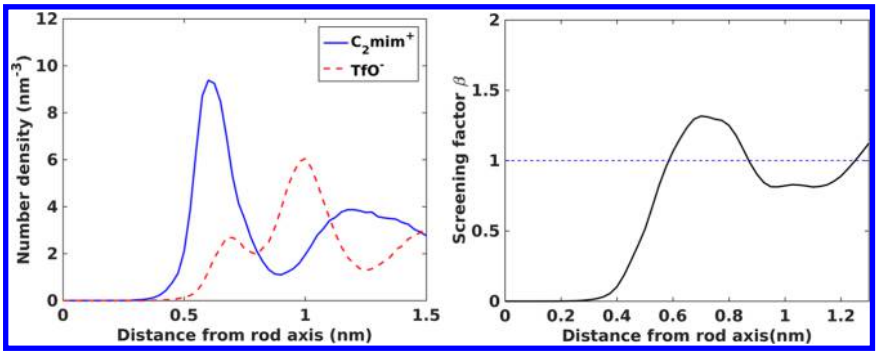

Figure 3. Ion density (a) and screening factor β (b) as a function of the radial distance from the PBDT rod axis in an ion gel. The positions of the C_2mim^+ and TfO^- ions are taken as atoms NE1 and ST in Figure 1a, respectively. The nominal rod spacing in the ion gel is 2.2 nm.

DOI: 10.1021/acs.langmuir.6b03798
Langmuir 2017, 33, 322−331

The structures of RTILs in ion gels with different nominal PBDT rod spacing are similar to those revealed in Figures 2 and 3a. In particular, as the rod spacing decreases from 2.8 to 2.0 nm, the amount of the C_2mim^+ and TfO^- ions in the first two ion layers near the PBDT rod only changes slightly (see Figure S4). To understand this, we note that the contact adsorption of C_2mim^+ ions on a PBDT rod is governed mostly by short-range electrostatic interactions with the sulfonate groups on this rod. Since these interactions are not greatly affected by the change of rod spacing (at least in the range explored here), the number of C_2mim^+ ions in contact with the sulfonate groups (and thus the PBDT rod) does not depend sensitively on the rod spacing. To see this quantitatively, we analyzed the density distribution of ions around the sulfonate groups in ion gels with different rod spacing and the results are shown in Figure 4. The sharp C_2mim^+ peak at r = 0.49 nm

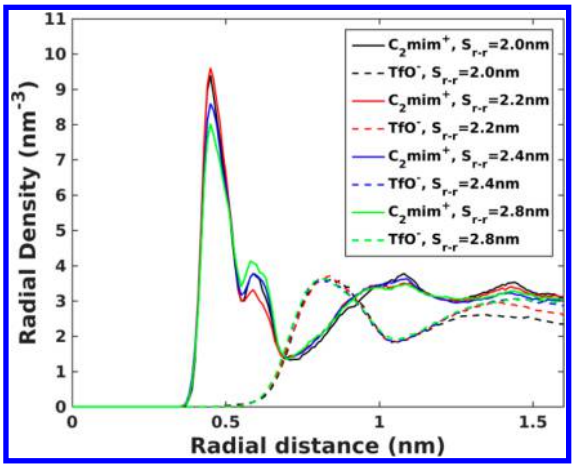

Figure 4. Radial density profiles of C_2mim^+ and TfO^- ions as a function of the ion distance to the sulfonate groups of the PBDT rod. The sulfur atom of the sulfonate group is taken as the origin.

indicates that each sulfonate group is coordinated (or "solvated") by several C_2mim^+ ions, and this coordination (or "solvation") changes weakly as the rod spacing varies.

Overall, the above results revealed that RTIL ions confined between PBDT rods are strongly heterogeneous and exhibit distinct structures at both inter-rod and smaller intermolecular scales. The structures at the inter-rod scale share key features of the RTIL structure near extended surfaces or within nanopores, but the chemical heterogeneity within each individual rod and the packing of PBDT rods also introduce new features into these structures. These correlated ion localizations form what we might call an "electrostatic network" that spans the entire ion gel, and which may give rise to the mechanical cohesion in this new class of ion gel materials.

3.2. Dynamics of Ionic Liquids in Ion Gels. *3.2.1. Basic Features.* Figure 5a shows the mean square displacement (MSD) curves of C_2mim^+ ions in bulk and in ion gels with a nominal rod spacing of 2.2 nm. The MSDs for ions in bulk liquids and in ion gels share some common features: all MSD curves exhibit three distinct regimes: the ballistic, subdiffusive, and diffusive regimes.[22] At the sub-picosecond time scale, a C_2mim^+ ion does not yet interact with its neighbors. It thus moves nearly ballistically and the MSD increases sharply with time. At a time scale of roughly 1 ps, the ion interacts with the ions surrounding it and its movement is hindered by the cage formed by neighboring molecules. Hence the MSD increases sublinearly, and the ion dynamics are subdiffusive. At a longer time scale (100−1000 ps and longer), the C_2mim^+ ion escapes the cage formed by its neighbors, and its MSD increases linearly with time as the ion dynamics reaches the diffusive regime.

Ion dynamics in these ion gels also show important differences from those in bulk liquids. First, the transition to the diffusive regime occurs at ∼2 ns in ion gels, much later than the ∼200 ps in bulk liquids. Second, ion diffusion is slower (a factor of 2−10) than in bulk liquids. Third, in line with experimental observations, the diffusion coefficient of C_2mim^+ ion in the direction along the rod ($D_\parallel$ = 3.6 × 10^{-11} m^2/s) is larger than in the direction across the rod ($D_\perp$ = 2.3 × 10^{-11} m^2/s). The first two observations originate from the association of C_2mim^+ ions with the sulfonate groups on the PBDT rod. As shown in Figure 4, several C_2mim^+ ions are in close contact with each sulfonate group. Since these C_2mim^+ ions are attracted to the sulfonate group quite strongly, they are hereafter called "sulfonate-associated ions". However, we note that any given associated cation will have a lifetime of approximately 5 ns on any given polymer-fixed SO_3^- anion (See Figure 6 below). This means that these associated cations

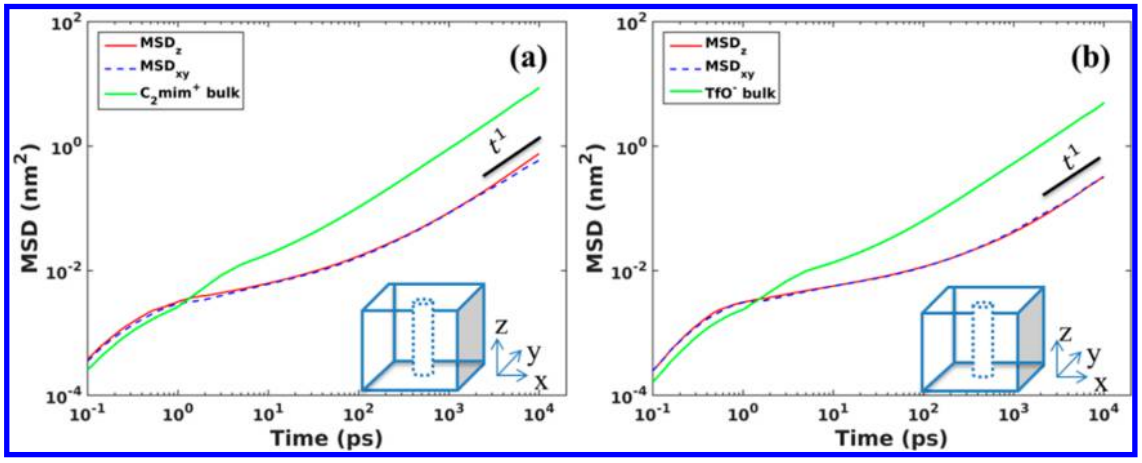

Figure 5. Mean-square-displacement (MSD) curves of C_2mim^+ (a) and TfO^- (b) ions in bulk and in ion gel with a nominal rod spacing of 2.2 nm. The *xy*-component of the MSD curves was divided by a factor of 2 to facilitate its comparison with the *z*-component of the MSD curves. In (a), the differences between the MSDs in the *xy*- and *z*-directions are not easily discerned in the log-scale plot. The differences between these MSDs are more easily observed in the linear scale plot shown in Figure S5.

DOI: 10.1021/acs.langmuir.6b03798
Langmuir 2017, 33, 322−331

are diffusing and exchanging with "free" cations on this relatively fast time scale.

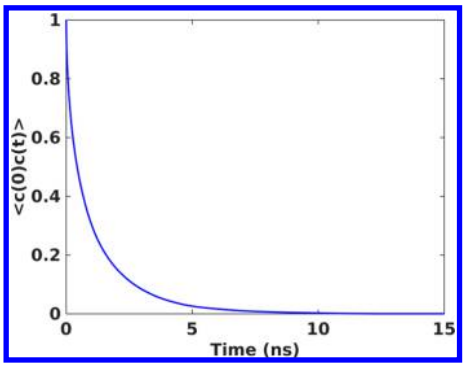

Figure 6. Time correlation function for the sulfonate-C_2mim^+ ion coordination in an ion gel with a nominal rod spacing of 2.2 nm.

To understand how the sulfonate-associated ions contribute to the first two observations, we note that any ion in a RTIL exists in the cage formed by its neighboring counterions.[21,46,47] The dynamics of an ion depends strongly on how easily the ion can escape its cage. For the sulfonate-associated C_2mim^+ ions, escaping their cage usually necessitates leaving the first coordinate shell of the sulfonate group. This is more difficult than C_2mim^+ ions escaping the coordination shell of their neighboring TfO^- ions in bulk liquids because the sulfonate group is nearly stationary while TfO^- ions in bulk liquids themselves diffuse randomly. Consequently, the transition of the MSD to diffusive regime is delayed and the diffusion is slower than in bulk liquids. To see how fast a sulfonate-associated C_2mim^+ ion escapes the coordination shell of its host sulfonate group, we computed the time correlation function for sulfonate-C_2mim^+ coordination

$$ACF_c(t) = \langle c(0)\, c(t)\rangle \tag{2}$$

where $c(t)$ is an indicator of the sulfonate-C_2mim^+ coordination. $c(t)$ is defined as 1.0 if a C_2mim^+ ion in the coordination shell of a sulfonate group (i.e., the first density peak in Figure 4) at time $t = 0$ is continuously coordinated to the sulfonate group by time t. Figure 6 shows that $ACF_c(t)$ decays to 0.1 in a few nanoseconds, which is similar to the time scale at which the MSD of C_2mim^+ ions in ion gels transition to the diffusive regime (see Figure 5a).

To confirm that sulfonate-associated C_2mim^+ ions contribute most significantly to the overall slow diffusion of the C_2mim^+ ions in the ion gel, we term the C_2mim^+ ions not in the coordination shell of any sulfonate group to be "free" ions. We then computed the self-part of the van Hove correlation function $G_s(r,t)$ for the sulfonate-associated ions and "free" C_2mim^+ ions using

$$G_s(r,\, t) = \frac{1}{N}\sum_{i=1}^{N}\langle\delta[\mathbf{r} + \mathbf{r}_i(0) - \mathbf{r}_i(t)]\rangle \tag{3}$$

where $\delta(\cdot)$ is the delta function, $\mathbf{r}_i$ is the position of ion i. The function $4\pi r^2 G_s(r,t)$ measures the probability that a particle has moved to a distance r away from its position at time $t = 0$. Figure 7 shows the function $4\pi r^2 G_s(r,t)$ for the sulfonate-associated and free C_2mim^+ ions in the ion gel at several time instants. Compared to those of the free ions, the peaks of $4\pi r^2 G_s(r,t)$ for the sulfonate-associated ions are narrower and shift systematically toward smaller distance r, thus confirming that these ions diffuse slower than the "free" ions.

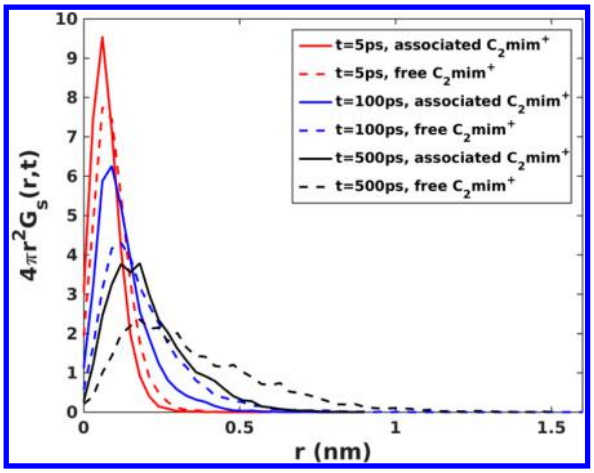

Figure 7. Self-part of the van Hove correlation function $4\pi r^2 G_s(r,t)$ for the sulfonate-associated and free C_2mim^+ ions in an ion gel with nominal rod spacing of 2.2 nm.

We also observe anisotropy of ion diffusion in the gel, which arises from several factors. First, due to hydrodynamic interactions, the hydrodynamic self-mobility of a particle adjacent to a planar surface is reduced compared to that in bulk fluids, and the reduction is more significant in the direction normal to the surface than parallel to the surface.[48] Such an effect, although expected to be weaker near PBDT rods due to their small radius, should still lead to a faster diffusion of ions parallel to the PBDT rod axis than normal to the PBDT rod. Second, the different pathways for ion transport along and across the rods also contribute to the anisotropy of the ion diffusion coefficient. Since the PBDT rods are well aligned, the movement of ions across the rods involves much more torturous pathways compared to that along the rods, leading to a smaller ion diffusion coefficient in the rod-perpendicular direction. This geometrical effect is further amplified by the presence of sulfonate-associated C_2mim^+ ions, which can associate with the sulfonate groups for a prolonged time period. As shown in Figure 8, these low-mobility ions create significant restrictions to ion diffusion perpendicular to the rods, thus enhancing diffusion anisotropy.

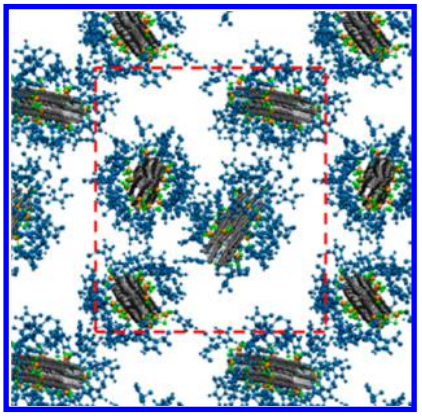

Figure 8. Top view snapshot of the ion gel with a nominal rod−rod spacing of 2.2 nm. The C_2mim^+ ions within the first coordination shell of the PBDT rod sulfonate groups are also shown. The red dashed lines denote the boundary of the simulation box.

DOI: 10.1021/acs.langmuir.6b03798
Langmuir 2017, 33, 322−331

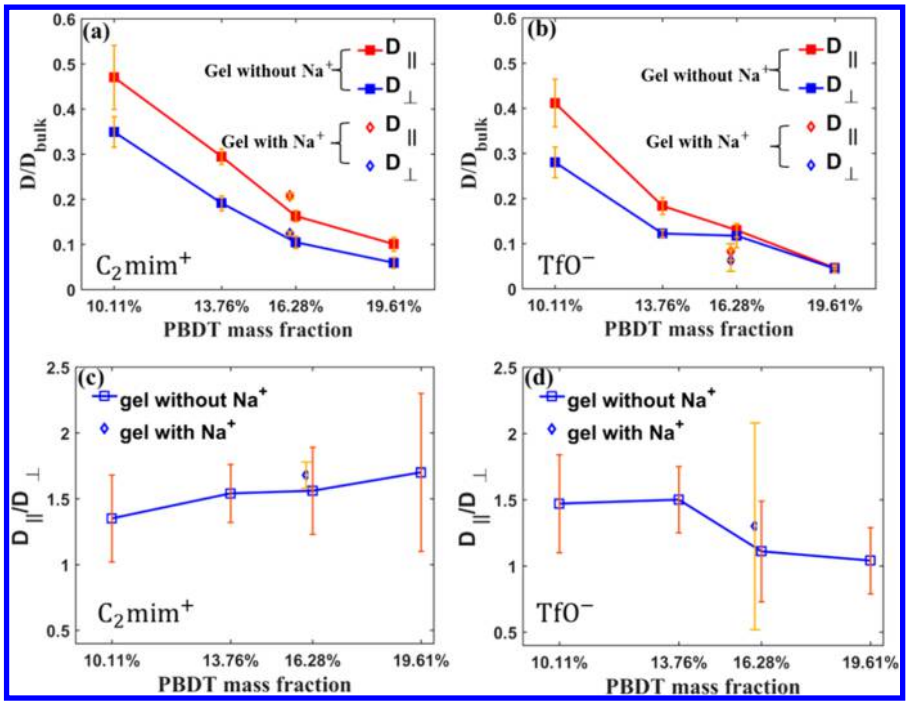

Figure 9. Diffusion coefficients of C_2mim^+ (a, c) and TfO^- (b, d) ions in ion gels with different PBDT mass fraction and residual Na^+ ions. Table 1 lists the nominal rod−rod spacing corresponding to the various PBDT mass fractions. The diffusion coefficients of the C_2mim^+ and TfO^- ions are 22.0×10^{-11} and 12.1×10^{-11} m^2/s in bulk $[C_2mim][TfO]$, respectively. Error bars are generated as described in section 2 (methods).

Thus far, we have examined only the dynamics of the C_2mim^+ ions in the ion gel. Figure 5b shows that the dynamics of the TfO^- ions exhibits similar features as the C_2mim^+ ions. That is, compared to those in bulk RTILs, the transition of the MSDs to the diffusive regime is delayed and the diffusion of the TfO^- ions is slower. These features are likely caused by the strong association of many TfO^- ions with the sulfonate-associated C_2mim^+ ions: Since the dynamics of the sulfonate-associated C_2mim^+ ions is sluggish, the TfO^- ions in their first coordinate shells will also be sluggish. In other words, cations and anions in the ion gel form an expansive, dynamic network due to the ion−ion electrostatic interactions. This "electrostatic network", already visible in the ion distribution shown in Figure 2, presumably contributes to the strong cohesion of the ion gel while also playing a fundamental role in the dynamics of ions. Importantly, many cations in this electrostatic network can become temporarily associated (~5 ns) with the stationary sulfonate groups of the PBDT rods, which tends to both anchor the electrostatic network and also slow down the dynamics of both cation and anions in the ion gel.

3.2.2. Effects of PBDT Loading. Figure 9 shows the effects of PBDT mass fraction (or equivalently, the nominal rod−rod spacing) on the diffusion coefficients of C_2mim^+ and TfO^- ions. The diffusion coefficients of C_2mim^+ and TfO^- ions are normalized using their respective bulk liquid values to better illustrate how rod−rod spacing affects the dynamics of these ions. Figure 9a shows that, $D_{\parallel}$ and $D_{\perp}$ of the C_2mim^+ ions decrease as the rod spacing decreases. We attribute this to the fact that, although the number of sulfonate-associated C_2mim^+ ions in the ion gel does not change greatly as the rod spacing decreases (cf. Figure 4), the fraction of sulfonate-associated C_2mim^+ ions increases. Since the sulfonate-associated C_2mim^+ ions diffuse slower than the "free" C_2mim^+ ions in the gel, the average diffusion coefficient of C_2mim^+ ions decreases. A similar decrease of diffusion coefficient is observed for the TfO^- ions (see Figure 9b). This is likely caused by the following factors. In the electrostatic network formed by C_2mim^+ and TfO^- ions that spans the entire ion gel, the dynamics of TfO^- ions are strongly correlated with that of the C_2mim^+ ions. Hence a slowdown of the dynamics of the C_2mim^+ ions at higher PBDT loading is accompanied by a slowdown of the dynamics of the TfO^- ions. Figure 9c and d shows that the anisotropy of ion diffusion in the gel is maintained in most of the gels studied here. However, a definite trend cannot yet be established due to the large statistical uncertainty of the data.

These MD simulations have captured the overall trends of the ion dynamics in ion gels, e.g., the decrease of ion diffusion coefficients as the PBDT loading increases and the notable diffusion anisotropy. However, some differences between simulations and experiment[16] do exist. The predicted slowdown of ion diffusion at increased PBDT loading is more significant than that measured experimentally. The predicted transport anisotropy is similar for C_2mim^+ and TfO^- ions, while experiments indicate a more distinct anisotropy for the TfO^- ions. These differences can originate from several sources. First, the force fields adopted here are parametrized for bulk liquids, and thus they may not capture the dynamics of RTILs confined in the highly heterogeneous environment in the ion gels. Second, the model adopted for the PBDT rods is relatively crude, although it captures some key features of the rods. Finally, experimentally, there are residual Na^+ ions in the ion gel, which are not taken into account in the above calculations. As shown below, these ions can significantly affect RTIL dynamics in the ion gel.

3.3. Structure and Dynamics of Ionic Liquids in Ion Gels with Residual Na^+ Ions. As discussed in section 2, some of the Na^+ ions in the aqueous PBDT seed solution used to prepare the ion gels remain in the dried gel.[16,33] To study how these Na^+ ions affect the structure and dynamics of RTILs in the gel, we built an ion gel with Na^+ ions. In the pre-

DOI: 10.1021/acs.langmuir.6b03798
Langmuir 2017, 33, 322−331

equilibration step, PBDT rods were fixed into a hexagonal lattice with a rod−rod spacing of 2.2 nm. Na^+ ions were first inserted between the PBDT rods to balance 50% of the charges on the PBDT rods, which is in line with the experimental observation that ∼50% of the Na^+ ions in the original seed solution are found to remain in the dried ion gels (see Supporting Information section 9). Next RTIL layers were placed at the two ends of the PBDT rods, and the pre-equilibration step proceeded as in the case for ion gels without Na^+ ions. This step was then followed by further equilibrium and production runs as described in section 2, during which the PBDT rods were allowed to move. Within the time scale (∼100 ns) examined here, all Na^+ ions stayed in the ion gel zone (denoted using a green box in Figure 1b), consistent with the counterion condensation effect found for PBDT solutions.[33] Therefore, Na^+ ions balance 50% of the negative charge on the PBDT rod, which is within the range found experimentally.

Figure 10 shows the ion distribution near the PBDT rods. We observe that Na^+ ions are concentrated near the surface of

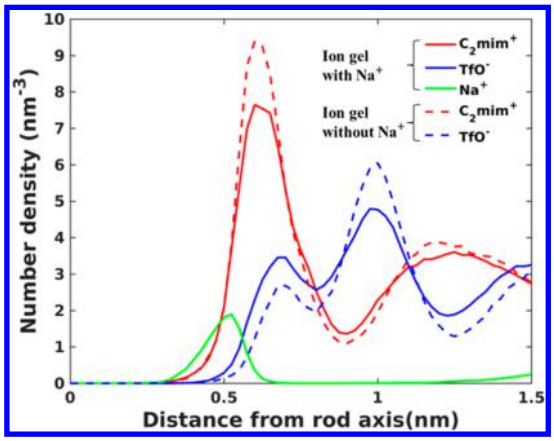

Figure 10. Ion density as a function of the radial distance from the axis of a PBDT rod in ion gels with and without residual Na^+ ions. Nominal rod spacing is 2.2 nm.

the PBDT rods. Compared to those in ion gels free of Na^+ ions, the height of the first C_2mim^+ peak decreases while that of the first TfO^- peak increases. Here we postulate that, because Na^+ ions are small, they are attracted toward the sulfonate groups of the PBDT rods more strongly than the bulky C_2mim^+ ions, thus displacing C_2mim^+ ions from the rod. The Na^+ ions adsorbed on the sulfonate groups in turn attract TfO^- toward the rod, leading to an enrichment of TfO^- near the rod. These postulations are corroborated by the calculations of the radial density distribution around the sulfonate groups. As shown in Figure S6, when Na^+ ions are introduced into the ion gel, they approach the sulfonate groups more closely than the C_2mim^+ ions. These Na^+ ions screen the electrostatic interactions between sulfonate groups and C_2mim^+ and TfO^- ions, which leads to a reduced coordination of the sulfonate groups by the C_2mim^+ ions and closer approach of the TfO^- ions toward the sulfonate group.

The change of RTIL structure in the gels induced by residual Na^+ ions leads to changes in RTIL dynamics (see Figure 9). Na^+ ions speed up the diffusion of the C_2mim^+ ions, which is consistent with the weakened association of C_2mim^+ ions with the PBDT rods (see Figure S6). Na^+ ions, however, slow down the diffusion of TfO^- ions in the gel. This is likely because TfO^- ions in the gel are more strongly coordinated with the less mobile Na^+ ions adsorbed on the PBDT rods. We propose to systematically test the effect of Na^+ concentration on the diffusion of C_2mim^+ and TfO^- ions in future experiments.

4. CONCLUSIONS

In summary, we have studied the structure and dynamics of $[C_2mim][TfO]$ in sulfonated aramid-based ion gels using MD simulations. This type of gel differs greatly from other polymer-based ion gels in that RTILs are dispersed between rigid, highly aligned, rod-like polyanions. The structure of RTILs in the ion gel exhibits features that are both unique to this ion gel as well as similar to ionic ordering near extended surfaces. For example, because of the discrete distribution of sulfonate groups and presence of hydrophobic domains on the PBDT rods, association of C_2mim^+ ions with the sulfonate groups of the PBDT rods and notable presence of anions on the surface of the negatively charged rods are observed. These RTIL structures can be modified to different extents by factors such as PBDT mass fraction (i.e., rod−rod spacing) and the presence of smaller inorganic ions in the gel. On the other hand, alternating layering of C_2mim^+ and TfO^- ions and charge overscreening, the hallmark of RTIL structure near charged surfaces, are also observed near the PBDT rods.

The RTIL dynamics predicted by our MD simulations agree qualitatively with that measured experimentally but some important differences exist. These differences may originate from the relatively simple models adopted in the present simulations. For example, the RTIL force fields are based on charge rescaling, which may not function well in the heterogeneous environment found in these ion gels. Likewise, the semi-coarse-grained rod model for the PBDT polyanions may not resolve important chemical details of these polyanions. In the future, RTIL force fields developed from first-principles[49] and all-atom models for PBDT polyanions need to be adopted to obtain a more accurate understanding of the structure and dynamics of RTILs in ion gels.

Since the distinct ordering of cations and anions both near the sulfonate groups and in the interstitial space between the PBDT rods are driven primarily by the electrostatic ion−ion interactions, we may view the heterogeneous structure formed by the ions as an "electrostatic network" that spans the entire gel. Such an electrostatic network, while far from being static, can impact greatly both the mechanical and transport properties of the ion gel. For example, the charge over screening underlying such a network likely contributes to the attraction between PBDT rods and thus to the mechanical cohesion and high modulus of the gel. Likewise, since some of the cations in the network are associated with the sulfonate groups of the PBDT rods, these associated ions tend to slow down the dynamics of the ions in the entire network. Even so, the ions on average diffuse quite fast ($D \sim 10^{-11}$ m^2/s) in these high modulus gels, showing promise for these materials to enable, e.g., high density Li-metal batteries.

Finally, we expect that specific molecular interactions, which vary substantially with IL chemical structure and are driven by, e.g., charge distribution and hydrophobicity, will strongly affect the final gel properties. RTIL correlations (nanometer-scale structuring) will influence both conductivity and modulus in these gels. For example, we expect that ILs with stronger correlations in time and space (as reflected in radial distribution functions and velocity autocorrelation functions) will drive the formation of higher modulus gels.

DOI: 10.1021/acs.langmuir.6b03798
Langmuir 2017, 33, 322−331

■ ASSOCIATED CONTENT

Supporting Information

The Supporting Information is available free of charge on the ACS Publications website at DOI: 10.1021/acs.langmuir.6b03798.

Molecular model and force field parameters for PBDT polyanions, distribution of C_2mim^+ and TfO^- ions around PBDT rods in ion gels with different PBDT loadings, the comparison of log-scale and linear-scale MSDs, the distribution of ions around sulfonate groups, and the experimental NMR measurements of the Na^+ concentration in as-fabricated ion gels (PDF)

■ AUTHOR INFORMATION

Corresponding Authors

*Email: ruiqiao@vt.edu (R.Q.).
*E-mail: lmadsen@vt.edu (L.A.M.).

ORCID

Rui Qiao: 0000-0001-5219-5530

Notes

The authors declare no competing financial interest.

■ ACKNOWLEDGMENTS

This work was partially supported by the US National Science Foundation under Award Numbers CBET 1264578 (Z.Y, Y.D.H., and R.Q.) and DMR 1507764 (Y.W. and L.A.M.). Any opinions, findings, and conclusions or recommendations expressed in this material are those of the author(s) and do not necessarily reflect the views of the National Science Foundation (NSF). The authors thank the ARC at Virginia Tech for generous allocation of computing time on the NewRiver and BlueRidge clusters.

■ REFERENCES

(1) Meyer, W. H. Polymer electrolytes for lithium-ion batteries. *Adv. Mater.* **1998**, *10*, 439−448.
(2) Wang, Y.-J.; Wilkinson, D. P.; Zhang, J. Noncarbon support materials for polymer electrolyte membrane fuel cell electrocatalysts. *Chem. Rev.* **2011**, *111*, 7625−7651.
(3) Lodge, T. P. A unique platform for materials design. *Science* **2008**, *321*, 50−51.
(4) Armand, M.; Endres, F.; MacFarlane, D. R.; Ohno, H.; Scrosati, B. Ionic-liquid materials for the electrochemical challenges of the future. *Nat. Mater.* **2009**, *8*, 621−629.
(5) Le Bideau, J.; Viau, L.; Vioux, A. Ionogels, ionic liquid based hybrid materials. *Chem. Soc. Rev.* **2011**, *40*, 907−25.
(6) Plechkova, N. V.; Seddon, K. R. Applications of ionic liquids in the chemical industry. *Chem. Soc. Rev.* **2008**, *37*, 123−150.
(7) Shi, R.; Wang, Y. Dual Ionic and Organic Nature of Ionic Liquids. *Sci. Rep.* **2016**, *6*, 19644.
(8) Zhang, Z.; Madsen, L. A. Observation of separate cation and anion electrophoretic mobilities in pure ionic liquids. *J. Chem. Phys.* **2014**, *140*, 084204−084213.
(9) Fedorov, M. V.; Kornyshev, A. A. Ionic liquids at electrified interfaces. *Chem. Rev.* **2014**, *114*, 2978−3036.
(10) Kubo, W.; Kambe, S.; Nakade, S.; Kitamura, T.; Hanabusa, K.; Wada, Y.; Yanagida, S. Photocurrent-determining processes in quasi-solid-state dye-sensitized solar cells using ionic gel electrolytes. *J. Phys. Chem. B* **2003**, *107*, 4374−4381.
(11) Hanabusa, K.; Fukui, H.; Suzuki, M.; Shirai, H. Specialist gelator for ionic liquids. *Langmuir* **2005**, *21*, 10383−10390.
(12) Lu, J.; Yan, F.; Texter, J. Advanced applications of ionic liquids in polymer science. *Prog. Polym. Sci.* **2009**, *34*, 431−448.
(13) Klingshirn, M. A.; Spear, S. K.; Subramanian, R.; Holbrey, J. D.; Huddleston, J. G.; Rogers, R. D. Gelation of ionic liquids using a cross-linked poly (ethylene glycol) gel matrix. *Chem. Mater.* **2004**, *16*, 3091−3097.
(14) Rupp, B.; Schmuck, M.; Balducci, A.; Winter, M.; Kern, W. Polymer electrolyte for lithium batteries based on photochemically crosslinked poly (ethylene oxide) and ionic liquid. *Eur. Polym. J.* **2008**, *44*, 2986−2990.
(15) Sun, T.; Wu, Z.; Gong, J. Self-assembled structures of a semi-rigid polyanion in aqueous solutions and hydrogels. *Sci. China: Chem.* **2012**, *55*, 735−742.
(16) Wang, Y.; Chen, Y.; Gao, J.; Yoon, H. G.; Jin, L.; Forsyth, M.; Dingemans, T. J.; Madsen, L. A. Highly Conductive and Thermally Stable Ion Gels with Tunable Anisotropy and Modulus. *Adv. Mater.* **2016**, *28*, 2571−2578.
(17) Wang, Y.; Jiang, W.; Yan, T.; Voth, G. A. Understanding ionic liquids through atomistic and coarse-grained molecular dynamics simulations. *Acc. Chem. Res.* **2007**, *40*, 1193−1199.
(18) Jiang, W.; Wang, Y.; Voth, G. A. Molecular dynamics simulation of nanostructural organization in ionic liquid/water mixtures. *J. Phys. Chem. B* **2007**, *111*, 4812−4818.
(19) Wang, Y.-L.; Lu, Z.-Y.; Laaksonen, A. Heterogeneous dynamics of ionic liquids in confined films with varied film thickness. *Phys. Chem. Chem. Phys.* **2014**, *16*, 20731−20740.
(20) Henritzi, P.; Bormuth, A.; Klameth, F.; Vogel, M. A molecular dynamics simulations study on the relations between dynamical heterogeneity, structural relaxation, and self-diffusion in viscous liquids. *J. Chem. Phys.* **2015**, *143*, 164502−164509.
(21) Del Pópolo, M. G.; Voth, G. A. On the structure and dynamics of ionic liquids. *J. Phys. Chem. B* **2004**, *108*, 1744−1752.
(22) Yan, T.; Wang, Y.; Knox, C. On the Dynamics of Ionic Liquids: Comparisons between Electronically Polarizable and Nonpolarizable Models II. *J. Phys. Chem. B* **2010**, *114*, 6886−6904.
(23) Rajput, N. N.; Monk, J.; Singh, R.; Hung, F. R. On the influence of pore size and pore loading on structural and dynamical heterogeneities of an ionic liquid confined in a slit nanopore. *J. Phys. Chem. C* **2012**, *116*, 5169−5181.
(24) Bazant, M. Z.; Storey, B. D.; Kornyshev, A. A. Double layer in ionic liquids: overscreening versus crowding. *Phys. Rev. Lett.* **2011**, *106*, 046102.
(25) Feng, G.; Zhang, J.; Qiao, R. Microstructure and capacitance of the electrical double layers at the interface of ionic liquids and planar electrodes. *J. Phys. Chem. C* **2009**, *113*, 4549−4559.
(26) Rajput, N. N.; Monk, J.; Hung, F. R. Structure and dynamics of an ionic liquid confined inside a charged slit graphitic nanopore. *J. Phys. Chem. C* **2012**, *116*, 14504−14513.
(27) Chaban, V. V.; Prezhdo, O. V. Nanoscale carbon greatly enhances mobility of a highly viscous ionic liquid. *ACS Nano* **2014**, *8*, 8190−8197.
(28) He, Y.; Qiao, R.; Vatamanu, J.; Borodin, O.; Bedrov, D.; Huang, J.; Sumpter, B. G. Importance of Ion Packing on the Dynamics of Ionic Liquids during Micropore Charging. *J. Phys. Chem. Lett.* **2016**, *7*, 36−42.
(29) Borodin, O. Polarizable force field development and molecular dynamics simulations of ionic liquids. *J. Phys. Chem. B* **2009**, *113*, 11463−11478.
(30) Costa, L. T.; Ribeiro, M. C. C. Molecular dynamics simulation of polymer electrolytes based on poly(ethylene oxide) and ionic liquids. II. Dynamical properties. *J. Chem. Phys.* **2007**, *127*, 164901−164907.
(31) Yan, T.; Burnham, C. J.; Del Pópolo, M. G.; Voth, G. A. Molecular dynamics simulation of ionic liquids: The effect of electronic polarizability. *J. Phys. Chem. B* **2004**, *108*, 11877−11881.
(32) Oza, Y. V.; MacFarlane, D. R.; Forsyth, M.; O'Dell, L. A. Characterisation of ion transport in sulfonate based ionomer systems containing lithium and quaternary ammonium cations. *Electrochim. Acta* **2015**, *175*, 80−86.

DOI: 10.1021/acs.langmuir.6b03798
Langmuir 2017, 33, 322−331

(33) Wang, Y.; Gao, J.; Dingemans, T. J.; Madsen, L. A. Molecular alignment and ion transport in rigid rod polyelectrolyte solutions. *Macromolecules* **2014**, *47*, 2984−2992.
(34) Zhong, X.; Liu, Z.; Cao, D. Improved classical united-atom force field for imidazolium-based ionic liquids: tetrafluoroborate, hexafluorophosphate, methylsulfate, trifluoromethylsulfonate, acetate, trifluoroacetate, and bis (trifluoromethylsulfonyl) amide. *J. Phys. Chem. B* **2011**, *115*, 10027−10040.
(35) Salanne, M. Simulations of room temperature ionic liquids: from polarizable to coarse-grained force fields. *Phys. Chem. Chem. Phys.* **2015**, *17*, 14270−14279.
(36) Schröder, C. Comparing reduced partial charge models with polarizable simulations of ionic liquids. *Phys. Chem. Chem. Phys.* **2012**, *14*, 3089−3102.
(37) Köddermann, T.; Paschek, D.; Ludwig, R. Molecular dynamic simulations of ionic liquids: A reliable description of structure, thermodynamics and dynamics. *ChemPhysChem* **2007**, *8*, 2464−2470.
(38) Berendsen, H. J.; van der Spoel, D.; van Drunen, R. GROMACS: a message-passing parallel molecular dynamics implementation. *Comput. Phys. Commun.* **1995**, *91*, 43−56.
(39) Hess, B.; Kutzner, C.; Van Der Spoel, D.; Lindahl, E. GROMACS 4: algorithms for highly efficient, load-balanced, and scalable molecular simulation. *J. Chem. Theory Comput.* **2008**, *4*, 435−447.
(40) Bussi, G.; Donadio, D.; Parrinello, M. Canonical sampling through velocity rescaling. *J. Chem. Phys.* **2007**, *126*, 014101−014108.
(41) Hess, B.; Bekker, H.; Berendsen, H. J.; Fraaije, J. G. LINCS: a linear constraint solver for molecular simulations. *J. Comput. Chem.* **1997**, *18*, 1463−1472.
(42) Yeh, I.-C.; Hummer, G. System-size dependence of diffusion coefficients and viscosities from molecular dynamics simulations with periodic boundary conditions. *J. Phys. Chem. B* **2004**, *108*, 15873−15879.
(43) Fedorov, M. V.; Kornyshev, A. A. Towards understanding the structure and capacitance of electrical double layer in ionic liquids. *Electrochim. Acta* **2008**, *53*, 6835−6840.
(44) Feng, G.; Qiao, R.; Huang, J.; Dai, S.; Sumpter, B. G.; Meunier, V. The importance of ion size and electrode curvature on electrical double layers in ionic liquids. *Phys. Chem. Chem. Phys.* **2011**, *13*, 1152−1161.
(45) Grosberg, A. Y.; Nguyen, T.; Shklovskii, B. Colloquium: the physics of charge inversion in chemical and biological systems. *Rev. Mod. Phys.* **2002**, *74*, 329−345.
(46) Wang, Y.; Voth, G. A. Tail aggregation and domain diffusion in ionic liquids. *J. Phys. Chem. B* **2006**, *110*, 18601−18608.
(47) Klaehn, M.; Seduraman, A.; Wu, P. A Model for Self-Diffusion of Guanidinium-Based Ionic Liquids: A Molecular Simulation Study. *J. Phys. Chem. B* **2008**, *112*, 13849−13861.
(48) Happel, J.; Brenner, H. *Low Reynolds Number Hydrodynamics*; Noordhoff Int. Publishing: Leyden, The Netherlands, 1973.
(49) Son, C. Y.; McDaniel, J. G.; Schmidt, J. R.; Cui, Q.; Yethiraj, A. First-Principles United Atom Force Field for the Ionic Liquid BMIM +BF4-: An Alternative to Charge Scaling. *J. Phys. Chem. B* **2016**, *120*, 3560−3568.

DOI: 10.1021/acs.langmuir.6b03798
Langmuir 2017, 33, 322−331